computation

MDPI

Article

Unraveling the Dual Inhibitory Mechanism of Compound 22ac: A Molecular Dynamics Investigation into ERK1 and ERK5 Inhibition in Cancer

Elliasu Y. Salifu [1,2,*], Mbuso A. Faya [2], James Abugri [3] and Pritika Ramharack [1,2,*]

[1] Biomedical Research and Innovation Platform (BRIP), South African Medical Research Council (SAMRC), Tygerberg 7505, South Africa
[2] School of Health Sciences, University of KwaZulu-Natal, Westville Campus, Durban 4001, South Africa; fayaa@ukzn.ac.za
[3] Department of Biochemistry and Forensic Sciences, School of Chemical and Biochemical Sciences, C. K. Tedam University of Science and Technology, Navrongo P.O. Box 24, Ghana; jabugri@cktutas.edu.gh
* Correspondence: elliasu.salifu@mrc.ac.za (E.Y.S.); pritika.ramharack@mrc.ac.za (P.R.)

Abstract: Cancer remains a major challenge in the field of medicine, necessitating innovative therapeutic strategies. Mitogen-activated protein kinase (MAPK) signaling pathways, particularly Extracellular Signal-Regulated Kinase 1 and 2 (ERK1/2), play pivotal roles in cancer pathogenesis. Recently, ERK5 (also known as MAPK7) has emerged as an attractive target due to its compensatory role in cancer progression upon termination of ERK1 signaling. This study explores the potential of Compound 22ac, a novel small molecule inhibitor, to simultaneously target both ERK1 and ERK5 in cancer cells. Using molecular dynamics simulations, we investigate the binding affinity, conformational dynamics, and stability of Compound 22ac when interacting with ERK1 and ERK5. Our results indicate that Compound 22ac forms strong interactions with key residues in the ATP-binding pocket of both ERK1 and ERK5, effectively inhibiting their catalytic activity. Furthermore, the simulations reveal subtle differences in the binding modes of Compound 22ac within the two kinases, shedding light on the dual inhibitory mechanism. This research not only elucidates a structural mechanism of action of Compound 22ac, but also highlights its potential as a promising therapeutic agent for cancer treatment. The dual inhibition of ERK1 and ERK5 by Compound 22ac offers a novel approach to disrupting the MAPK signaling cascade, thereby hindering cancer progression. These findings may contribute to the development of targeted therapies that could improve the prognosis for cancer patients.

Keywords: MAPK; cancer; catalytic activity; molecular dynamics; pathogenesis

Citation: Salifu, E.Y.; Faya, M.A.; Abugri, J.; Ramharack, P. Unraveling the Dual Inhibitory Mechanism of Compound 22ac: A Molecular Dynamics Investigation into ERK1 and ERK5 Inhibition in Cancer. *Computation* **2024**, *12*, 45. https://doi.org/10.3390/computation12030045

Academic Editor: Francesco Cauteruccio

Received: 19 December 2023
Revised: 28 January 2024
Accepted: 14 February 2024
Published: 1 March 2024

1. Introduction

The intracellular communication within eukaryotic cells is orchestrated by an intricate network of signaling pathways, which play a fundamental role in regulating various cellular processes, including growth, differentiation, proliferation, and responses to external stimuli [1–5]. Among the many intracellular signal transduction pathways in cancer pathogenesis and tumorigenesis, mitogen-activated protein kinases (MAPKs) have been shown to play a significant role due to their key contributions in the regulation of a wide array of cell-mediated processes including cellular differentiation, mitosis, proliferation, cellular responses to stress, metastases, angiogenesis, apoptosis, and senescence [6–11]. The MAPK signaling cascade is a complex and highly conserved intracellular signaling pathway found in eukaryotic cells. It plays a crucial role in transmitting extracellular signals to the nucleus, where it regulates a wide range of cellular processes. The MAPK cellular signaling cascade in eukaryotes has been categorized into four main groups, namely, the p38 MAPK signaling cascade, the c-Jun amino-terminal (JNK) MAPK signaling cascade (also referred to

as stress-activated protein kinases), the extracellular signal-regulated kinase 1 and 2 (ERK1 and ERK2) MAPK signaling cascade (also known as classical MAPK), and the extracellular signal-regulated kinase 5 (ERK5) signaling cascade (also referred to as the big MAPK or BMK1) [12–19].

Extracellular signal-regulated kinases (ERKs) are ubiquitously expressed and are the most studied MAPK families, mainly for their roles in pathological conditions, especially cancer, osteoporosis, arthritis, and inflammation [20–22]. ERK classification includes the "classical" group consisting of the serine–threonine kinases, ERK1 (p44 MAPK) and ERK2 (p42 MAPK), believed to share highly similar amino acid sequences [23]; the "atypical" group consisting of ERK3, ERK4, ERK7, and ERK8 which, although possessing overlapping sequence similarity with ERK1/2 follow upstream phosphorylation through members of MAPKs [23,24]; and the relatively unknown dual protein kinase-transcription factor, ERK5 [24].

In the work of Wang et al., 2020 [25], the up-regulation and increased expression of genes coding for both ERK1 and ERK5 were observed in some forms of cancer including kidney renal clear cell carcinoma, liver hepatocellular carcinoma, cholangiocarcinoma, and acute myeloid leukemia [26]. Considerably high domain similarity has been reported for both ERK1 and ERK5, notably at their ATP-binding sites, which would pre-empt similarities in biological functions [27,28]. They are both activated by growth factors, phosphorylate substrates like c-Myc and RSK, induce the similar early genes c-Jun and c-Fos, and control cell proliferation and differentiation [29]. Other researchers have also identified varying contributions either in terms of direct implication or mutation of chemotherapeutic agents played by ERK1 and ERK5 in colorectal cancer [30], breast cancer [31,32], prostate cancer [33], lung cancer [34–36], GIT sarcoma [37], glioblastoma [38], and liver cancer [39].

While ERK1 has been shown experimentally to be a major oncogenic driver in intestinal epithelial cells [40–44], both genetic deletion and clinical inhibition of the function of this family of MAPK have revealed a supraphysiological expression of the activity of ERK5 (whose up-regulation has been documented in a wide array of diseases including various forms of cancer [45–48]). This indicates that ERK5 could provide an alternative route for the persistent pathological expression of ERK1-related endogenous functions [26]. It is, therefore, hypothesized that drug discovery and drug developmental efforts geared toward dual inhibition of both ERK1 and ERK5 may provide a novel and significantly improved pharmacologic alternative to currently available MAPK inhibitors.

Although various selective inhibitors of the ERK1 proteins have been investigated against some forms of cancer including BVD-523, GDC0994, and SCH772984, and XMD8-92 has been documented to be effective against the ERK5 protein, none of these agents possess an intrinsic capacity for dual activity against ERK1 and ERK5, as stated in our hypothesis. However, a novel compound, 2-(2-Chlorobenzamido)-6-((2-chlorophenyl)carbamothioyl)-4,5,6,7-tetrahydrothieno [2,3-c]pyridine-3-carboxamide (Compound 22ac) (Figure 1), was recently synthesized and identified as an ERK1/ERK5 dual-inhibitor, where the inhibitor is believed to possess the ability to bind to the ATP-competitive hinge binding site of both proteins. *In vitro* experiments by Guan et al. in 2020 revealed that compound 22ac exhibits effective anti-proliferative activity. Additionally, according to kinase inhibitory assays, the IC50 values for ERK1 and ERK5 were determined to be 40.43 nM and 64.50 nM, respectively [26]. These findings establish Compound 22ac as a potent dual inhibitor for both ERK1 and ERK5. The results from *in vivo* experiments demonstrated that administering Compound 22ac orally at a dose of 50 mg/kg once daily for 16 days led to a significant reduction in tumor volume in a xenograft mouse model involving HL-60 and MKN-74 cells, as reported by Guan et al. in 2020 [26]. In this study, we set out to investigate, and subsequently provide atomistic insights into the mechanism of dual-target inhibition of both ERK1 and ERK5 by Compound 22ac using a molecular dynamic simulation technique.

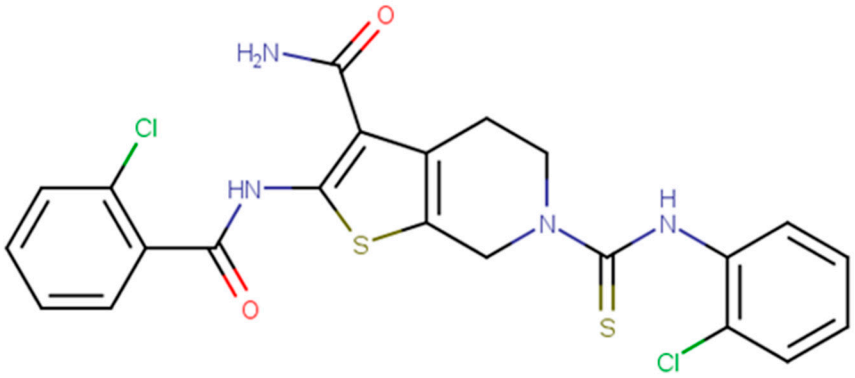

Figure 1. The 2-dimensional structure of Compound 22ac using MarvinSketch version 6.3.0. Coloring highlights the different elements in the structure.

2. Materials and Methods

2.1. System Preparation

The RCSB Protein Data Bank was assessed to retrieve X-ray crystal structures of ERK1 and ERK5 with the respective PDB codes of 4QTB and 4B99 [26]. The retrieved structures were solved via X-ray diffraction at resolutions less than 3.0 Å. The structures were then prepared for molecular docking using the graphical user interface of UCSF Chimera version 1.12, where all non-standard amino residues including water, ions, salts, and native inhibitors were removed from the protein structures to reduce computational cost [49]. The native inhibitors were used to define the active site region by highlighting all amino acid residues that lie with 5 Å from the compound. Additionally, the integrated MODELLER plugin [50] in Chimera software was used to model and refine all missing amino acid residues on both enzymes [51]. The 2D structure of Compound 22ac was drawn on MarvinSketch version 6.3.0 [52] and optimized in a 3D format using Avogadro software version 1.2.0 [53]. To serve as control molecules, the structures of SCH772984 and XMD8-92, two known inhibitors specific to ERK1 and ERK5, respectively, were retrieved from PubChem [54]. Subsequently, molecular docking was carried out for each enzyme against Compound 22ac using AutoDock Vina version 1.1.2 [55], an integrated tool for molecular docking on UCSF Chimera version 1.12 software [49]. The best binding score and pose of Compound 22ac in the active site of each enzyme were selected as initial structures of the molecular dynamics (MD) simulation. A total of six (6) systems were set up for MD simulation, comprising the Unbound structures of ERK1 (apo) and ERK5 (apo) and the complex structures of ERK1-Compound 22a, ERK1-SCH772984, ERK5-Compound 22a, and ERK5-XMD8-92.

2.2. Molecular Docking and Molecular Dynamics (MD) Simulations

The prepared systems were subjected to 200 ns MD simulations run via the graphic processor unit (GPU) of AMBER18 with an integrated LEAP module and PMEMD engine [56]. Using the ANTECHAMBER program, partial charges were generated for the ligand with the use of general amber force field (gaff) bcc charge. With the AMBER force fields, leaprc.gaff and leaprc.ff14SB, the ligands and proteins were parameterized, respectively [57]. The pdb4amber script was used to protonate histidine at a constant pH in order to automatically modify the protein before running the LEAP module. The LEAP module added all missing atoms of hydrogen as well as the counter ions for neutralization, and consequently, topology and coordinate files for the ligand, protein, and complex were generated [58]. Systems were made to solvate in cubic boxes filled with TIP3P water molecules with box-sized 10 Å [59]. With a restraint of 500 kcal/molÅ potential, 2500 steps of partial minimization were achieved, and with 1000 steps, full minimization with no restraint was then performed. Gradual heating from 0 to 300 k of the systems was carried out during 50 ps. Also, with Berendsen barostat, the systems were equilibrated at a temperature of 300 k and 1 bar pressure for 500 ps [60]. MD simulation was implemented for 200 ns in a

1 fs time step, and the trajectories were saved in every 1 ps. Coordinates and trajectories were generated and saved for further analysis with the aid of the PTRAJ and CPPTRAJ modules in AMBER18 [61]. Plots were obtained by Microcal Origin analysis software version 6.0 [62], while both visual and structural analyses were performed using UCSF Chimera version 1.12 [49]. Conformational dynamics such as the root mean square deviation (RMSD), root mean squared fluctuation (RMSF), and radius of gyration (RoG) were analyzed.

2.3. Molecular Mechanics Generalized Born Surface Area (MM/GBSA)

Molecular Mechanics Generalized Born Surface Area was used to calculate the binding free energy of the 22ac, SCH772984, and XMD8-92 complexes [63]. The energy estimate helps to predict the affinity and binding strength of a small compound to the binding pocket of a protein target. MM/GBSA is represented mathematically below:

$$\Delta G_{bind} = G_{complex} - (G_{ligand} + G_{receptor})$$

$$E_{gas} = E_{ele} + E_{int} + E_{vdw}$$

$$G_{sol} = G_{PB} + G_{SA}$$

$$G_{SA} = \gamma SASA$$

$$G_{sol} = G_{PB} + \gamma SASA$$

where $E_{gas,}$ a summation of internal energy (E_{int}), represents the energy at the gas phase, while E_{ele} and E_{vdw} are electrostatic and van der Waals energies, respectively. G_{sol} represents solvation-free energy, which is the summation of polar solvation (G_{PB}) and non-polar solvation (G_{SA}). G_{SA} is determined by SASA, the solvent-accessible surface area, by means of a water probe radius of 1.4 Å and a 0.0072 kcal/(mol·Å^2) surface tension constant (γ).

3. Results

3.1. Characterization of Inhibitors Using Online Predictive Databases

Absorption, distribution, metabolism, and excretion (ADME) highlight the physiological processes that a drug undergoes in the body. ADME and toxicity assessments are crucial steps in the drug development process. Understanding these processes is essential for developing safe and effective drugs. The ADME characterization of Compound 22ac, SCH-772984, and XMD8-92 was predicted via the SWISSADME database. SWISSADME is a website developed by the Swiss Institute of Bioinformatics to predict the pharmacokinetics, drug-likeness, and chemistry-friendliness of small molecules. As shown in Table 1, the Lipinski rule of five was considered in assessing the drug-likeness of the selected compounds. Also, the synthetic accessibility was predicted to highlight how easily each molecule can be experimentally synthesized. The findings show the diverse properties among the selected dual inhibitors of ERK1 and ERK5. The molecule of interest, Compound 22ac, had a molecular weight (505.44 kg/mol) above the recommended standard (500 kg/mol) according to the rule of five. Similarly, SCH-772984 showed a higher molecular weight (587.67 kg/mol) above the standard of the rule of five. XMD8-92, on the other hand, complied with the rule of five. However, all compounds show moderate solubility in water and have good lipophilic properties, highlighting their ability to permeate the lipid membrane as well as dissolve in fatty acids and oils. Additionally, the synthetic accessibility score indicated that XMD8-92 can be easily synthesized, followed by Compound 22ac and then SCH-772984. This parameter is determined by a scale ranging from 1 (very easy to synthesize) to 10 (very difficult to synthesize) [64]. Also, the compounds were assessed to determine whether they were inhibitors or substrates of P-glycoprotein, which has an excretory role. SCH-772984 and XMD8-92 were predicted to be substrates of the P-gp enzymes, while Compound 22ac was identified as not being a substrate of the P-gp enzyme. Conversely, SCH-772984 and Compound 22ac were predicted to be inhibitors of CYP34A, while the result indicated that

XMD8-92 was not a CYP3A4 inhibitor. These findings highlight the metabolic properties of these ERK inhibitors.

Table 1. ADME and toxicity assessment of inhibitors of ERK1 and ERK5.

Property	Compound		
	SCH-772984	XMD8-92	Compound 22ac
Molecular weight g/mol	587.67	474.55	505.44
H-bond donors	2	2	2
H-bond acceptors	7	5	3
Lipophilicity (ILOGP)	2.62	3.95	3.09
Solubility (ESOL)	Moderate	Moderate	Moderate
GI absorption	High	High	Low
Synthetic accessibility	4.38	3.63	3.65
Lipinski rule	Yes, two violations	No	Yes, one violation
P-gp substrate	Yes	Yes	No
CYP1A2 inhibitor	No	No	No
CYP2C19 inhibitor	Yes	Yes	Yes
CYP2C9 inhibitor	Yes	Yes	Yes
CYP2D6 inhibitor	Yes	Yes	No
CYP3A4 inhibitor	Yes	No	Yes
LD50 (mg/Kg)	419	1500	1200
Toxicity class	4	4	4
Hepatotoxicity	Inactive	Inactive	Inactive
Immunotoxicity	Active	Active	Inactive
Mutagenicity	Inactive	Inactive	Inactive
Cytotoxicity	Active	Active	Inactive
Carcinogenicity	Active	Inactive	Inactive

The toxicity prediction shows that all inhibitors were in toxicity class four (4), indicative of less toxicity when swallowed. SCH-772984 was active toward endpoints like immunotoxicity, cytotoxicity, and carcinogenicity, indicating that when administered above the lethal dosage, it may be toxic toward these endpoints. XMD was also active toward endpoints like immunotoxicity and carcinogenicity. Compound 22ac did not show any toxic effects toward any of the selected endpoints.

3.2. Structural Similarity in ERK1 and ERK5 Surrounding Dual Targeting by Compound 22ac

ERK1 and ERK5, two members of the extracellular signal-regulated kinase (ERK) family, show structural and functional similarities. These kinases share a distinct resemblance, with a sequence identity of approximately 44.47%. Furthermore, a closer examination of their kinase domains reveals a sequence identity of approximately 66% within this critical region. Both ERK1 and ERK5 display a characteristic Thr-Glu-Tyr motif in their activation loops, which serves as a pivotal site for dual phosphorylation [65]. This shared motif underscores their functional commonalities and the conservation of their activation mechanisms. Also, they both house a conserved phosphate binding loop (P-loop) that is essential for ATP binding, auto-phosphorylation, and substrate recognition, which are important for the function of the ERK signaling cascade. There is also the DFG domain, which is critical for regulating the kinase activation and deactivation states.

The substantial degree of sequence homology between ERK1 and ERK5 suggests a strong likelihood of shared interactions with common ligands. It is a well-established principle that structurally similar receptors are more likely to bind similar ligands. Therefore, the notable sequence homology observed in these kinases not only highlights their evolutionary relationship but also implies a shared range of ligands or signaling partners. This convergence in sequence and functional motifs further underscores the significance of ERK1 and ERK5 in mediating cellular responses to various extracellular signals, making them key players in signal transduction pathways. The structural alignment of the

two proteins after molecular docking with Compound 22ac show the following conserved residues at the active site: Ile61-Gly67, Val69, Ala82, Lys84, Glu102, Ile115, Leu137-Asp143, His145, Gln146, Lys184, Ser186, Asn187, Leu189, Gly199, and Asp200 of the ERK5 structure, while the implicated residues in the ERK1 protein include: Ile48-Gly51, Tyr53, Val56, Ser57, Ala69, Lys71, Ile73, Glu88, Ile101, Glu122-Lys131, Lys168, Ser170, Asn171, Leu173, Cys183, and Asp184, as shown Figure 2.

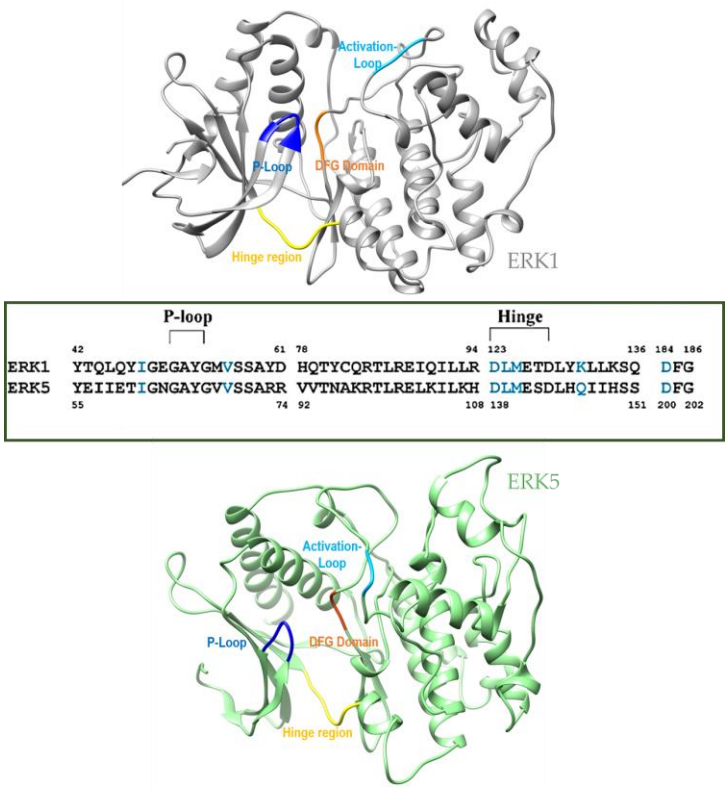

Figure 2. Structural comparison of ERK and ERK5 showing identical residues and important domains that highlight enzyme activity.

3.3. Structural Stability of the Simulated Systems

Ligand binding can induce conformational changes in a protein, and these changes can be influenced by artifacts in the simulation. Artifacts may stabilize or destabilize certain protein conformations, leading to differences in the conformational dynamics observed between the bound and unbound states. Protein stability is directly measured using the root mean square deviation (RMSD) and the radius of gyration (RoG) of the C-α atoms of the backbone. While a high RMSD value could directly be linked to an unstable system that requires a longer simulation time, a low RMSD value consequently means that the simulated system is relatively stable [66]. As shown in the Figure 3, the system was run for a total simulation period of 200 ns, where the stability of the system was observed.

It can be seen from the plot of both the unbound and bound systems that the ligands exhibited relatively stable conformation along the two receptors. In ERK1, the unbound system had a mean value of 1.90 Å, while the bound system in complex with Compound 22a, SCH-772984, and XMD8-92 had mean values of 1.40 Å, 1.86 Å, and 1.72 Å, respectively. Interestingly, a similar trend of stable systems was seen in the ERK5 system where the unbound system had a mean value of 2.19 Å, while the bound systems had mean values of 1.94 Å, 2.30 Å, and 2.40 Å. The Compound 22a-bound systems showed the lowest RMSD values in both ERK1 and ERK5, highlighting it as slightly more stable on each enzyme as compared with the other two reference inhibitors. RoG estimations show similar structural compactness of the bound and unbound systems.

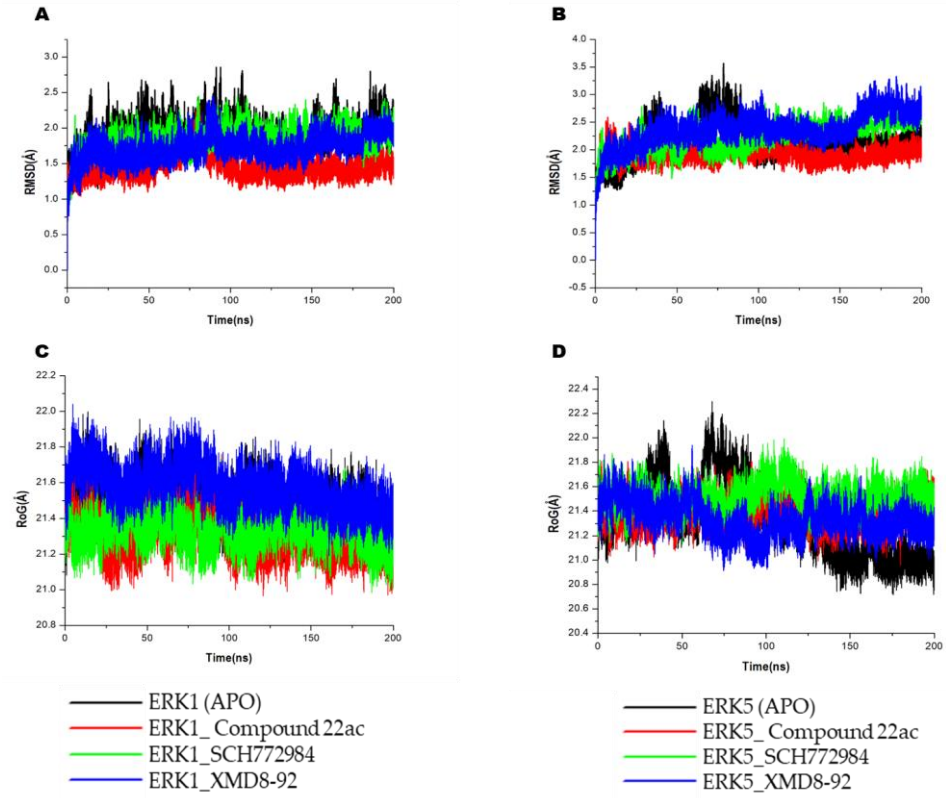

Figure 3. Conformational analysis plot of whole system RMSD showing stability and atomistic motions of (**A**) ERK1 and (**B**) ERK5. Also shown is the RoG plot, which estimates the relative compactness of the systems for (**C**) ERK1 (**D**) ERK5. Systems are either unbound (APO) or complexed with compound 22ac (red), SCH772984 (green), or XMD8-92 (blue).

RoG is one of the most important markers for unraveling a macromolecule's structural activity and indicates the changes in complex compactness. Therefore, the stability of apo enzymes, Compound 22a, SCH-772984, and XMD8-92 in complex with EKR1 and ERK5 enzymes were also analyzed in terms of RoG over a 200 ns simulation time, as shown in Figure 2. The average RoG in the ERK1 systems was found to be 21.47 Å, 21.30 Å, 21.32 Å, and 21.57 Å for the apo ERK1-, Compound 22a-, SCH-772984-, and XMD8-92-bound complexes, respectively, indicating the active site of the protein does not induce major conformational changes after binding the inhibitors. While in the ERK5 systems, the RoG was estimated to be 21.27 Å, 21.42 Å, 21.351 Å, and 21.32 Å for the apo ERK1-, Compound 22a-, SCH-772984-, and XMD8-92-bound complexes, respectively, indicating a similar conformational effect of inhibitors on ERK5.

3.4. Impact of Compound 22ac, SCH-772984, and XMD8-92 on Structural Flexibility

Structural flexibility was analyzed by estimating the root mean square fluctuation (RMSF) to give insights into the flexibility of the amino acid residues in the bound and unbound protein structures. The RMSF can help to characterize and estimate the local changes within the protein structure as a result of inhibitor binding during the simulation. Therefore, the mean RMSF values of the simulated systems were calculated to observe the change in structural flexibility of the protein during binding of the inhibitors to specific residual positions. The mean RMSF values for the unbound and bound systems for ERK1 were 0.90 Å, 0.91 Å, 0.89 Å, and 0.93 Å for apo ERK1-, Compound 22a-, SCH-772984-, and XMD8-92-bound complexes, respectively, while in ERK5 system, the mean value for the unbound and bound system were 1.31 Å, 1.16 Å, 1.07 Å and 1.01 Å for the apo ERK5-, Compound 22a-, SCH-772984-, and XMD8-92-bound complexes, respectively. There were minimal atomistic fluctuations at the hinge regions of both the ERK1 and ERK5 complexes.

Similarly, there were no significant fluctuations in the P-loop region (Gly51-Gly54) of ERK1 or the ERK5 loop regions (Gly64-Gly67). Notably, peak fluctuations were observed at positions Gly51, Asn175, Tyr250, Met350, and Gly374 in the ERK1-bound systems including the apo system as shown in Figure 4. Similarly, in the ERK5 systems, peak fluctuation regions were observed at Asp50-Arg75, Asp200-Trp226, and Met275-Gly315. We can observe that during the simulation time, the amino acid residues of unbound ERK1 and ERK5 had similar structural motions as the inhibitor-bound systems, which indicates that the inhibitors did not have a significant impact on the flexibility of the targets.

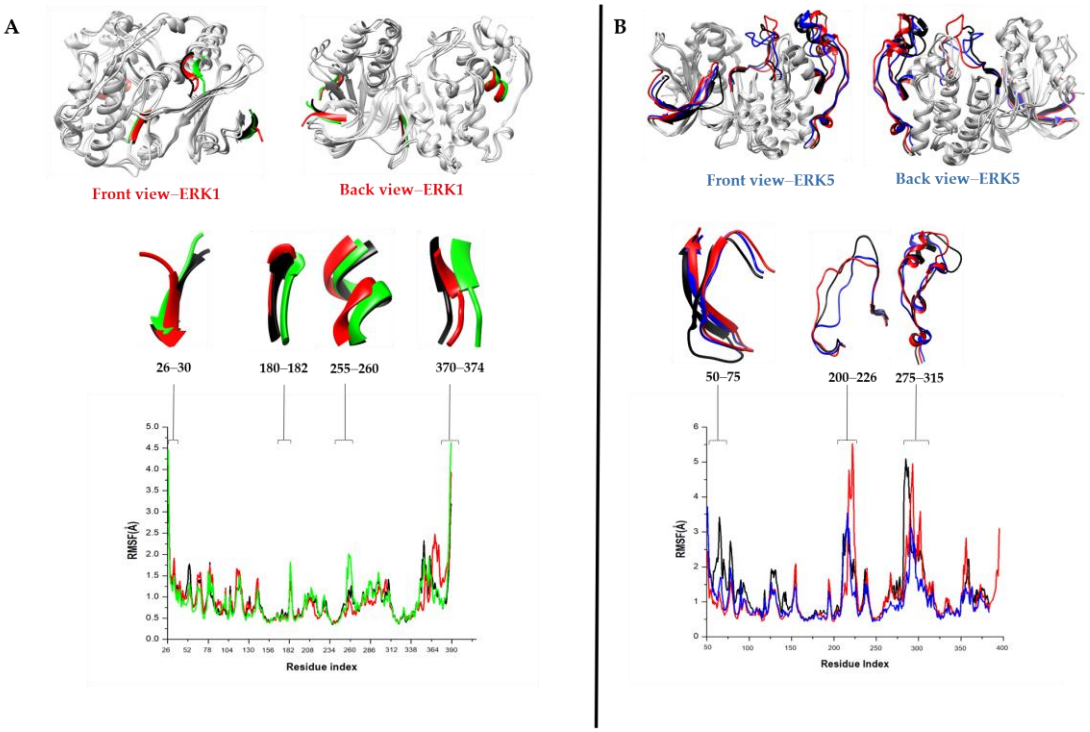

Figure 4. Comparative RMSF plots showing the degree of residual fluctuations of the (**A**) ERK1 and (**B**) ERK5 proteins upon binding by Compound 22ac over the 200 ns MD simulation time. Also shown are the peak regions of the fluctuations in the protein structure during the simulation.

3.5. Binding Free Energy Calculation and Per-Residue Energy Contributions of Compound 22ac, SCH-772984, and XMD8-923

Binding Free Energy Calculations for Both Ligand–Protein Complexes

The molecular dynamics trajectories obtained from the protein–ligand complexes of ERK1 and ERK5 bound to Compound 22ac, SCH-772984, and XMD8-92 were used to calculate binding free energy using the Poisson–Boltzmann (PB) implicit solvent method based on solvent accessible surface area (SASA) [63]. The MM/GBSA method is widely used in a range of applications including protein–protein interactions, conformational stability of ligand–protein complexes, and in re-scoring [67]. A total of 200 snapshots were extracted at equal intervals from the equilibrated time frame of 100 ns–200 ns of the MD trajectories for binding energy estimation. The different energy terms linked with binding free energies are tabulated in Table 2.

The findings show that the protein–ligand complexes had high negative free energy values, indicative of optimal binding of all three ligands to the target enzymes. The combined estimated energies ranged from −34.53 kcal/mol to −61.12 kcal/mol for all complexes. SCH-772984 bound the strongest (−61.12 kcal/mol) to the ERK1 enzyme as compared with Compound 22ac, which showed the least binding energy (−34.53 kcal/mol) toward ERK1. Similarly, in the ERK5-bound systems, Compound 22ac showed a slightly higher binding free energy as compared with the specific ERK5 inhibitor XMD8-92, as

shown in Table 2. Compound 22ac was shown to slightly bind favorably toward ERK5 (−35.53 kcal/mol) in contrast to its binding toward ERK1. Overall, Compound 22ac displayed good affinity and the capability to have considerable activity at the ATP hinge-binding sites of both enzymes, and this may therefore explain its dual-inhibitory potential against the target enzymes. Despite the high unfavorable polar solvation energy displayed across all the protein–ligand complex systems, the relatively high van der Waals forces (ΔE_{VDW}), electrostatic energy (ΔE_{ele}), and gas phase (ΔE_{gas}) ensured that the total binding free energy for the protein–ligand complex remained favorable. The van der Waals forces (ΔE_{VDW}), electrostatic energy (ΔE_{ele}), and gas phase (ΔE_{gas}) were thus the favorable energy terms that contributed to the favorable binding of the dual inhibitors for both enzymes.

Table 2. Binding free energy calculation of inhibitors against the ERK1 and ERK5 enzymes.

Complex	ΔE_{ele}	ΔE_{vdw}	ΔE_{gas}	ΔE_{sol}	ΔE_{bind}
	Energy Contributions (kcal/mol)				
ERK1-Compound 22a	−20.38 ± 0.36	−44.02 ± 0.26	−64.40 ± 0.47	29.88 ± 0.28	−34.53 ± 0.32
ERK5-Compound 22a	−35.41 ± 0.36	−46.64 ± 0.36	−82.05 ± 0.88	46.51 ± 0.72	−35.53 ± 0.42
ERK1-SCH	−107.90 ± 1.19	−58.19 ± 0.36	−166.09 ± 1.17	104.97 ± 1.18	−61.12 ± 0.46
ERK5-XMD	−10.81 ± 0.58	−48.06 ± 0.44	−58.87 ± 0.80	23.78 ± 0.57	−35.09 ± 0.44

ΔE_{ele} = electrostatic energy; ΔE_{vdw}. = van der Waals energy; ΔE_{gas} = gas phase free energy; ΔE_{sol}. = solvation free energy; ΔE_{bind} = total binding free energy.

3.6. Per-Residue Energy Contributions of the ERK1-Compound 22a and ERK5-Compound 22a Complexes

To gain further insights into the binding energetics of the simulated systems, the per residue energy decomposition technique was used. Per-residue energy decomposition is a computational method for analyzing the contributions of individual amino acid residues or other components to the overall energy of a molecular system. This technique is particularly valuable for understanding the molecular interactions and energetics driving protein–ligand binding. To this effect, residual energy contributions as well as interactions were calculated via the MM/GBSA method and ligplus software (version 2.2) respectively, to identify crucial amino acids that play an important role in the binding of the inhibitors. This calculation considers various energy terms, such as van der Waals interactions, electrostatic interactions, hydrogen bonding, and solvation energies, which contribute to the overall energy of the system. Compound 22ac was observed to bind to the following high-energy contributing amino acid residues in the active site of ERK1: Tyr53, Val56, Lys168, Ser170, Leu173, and Asp184, as shown in Figure 5. Val56 was also noted to form a hydrogen bond interaction in addition to its high energy contribution toward the final binding energy of the complex. Also, Ile61, Val69, Ser142, Leu189, Lys84, and Glu141 residues were identified as the high-energy contributing residues in the ERK5_Compound 22a complex system, with Lys84 and Glu141 forming hydrogen bonds with Compound 22a. Similarly, important residues contributing to the binding of SCH-772984 and XMD8-92 are highlighted in Figure S1.

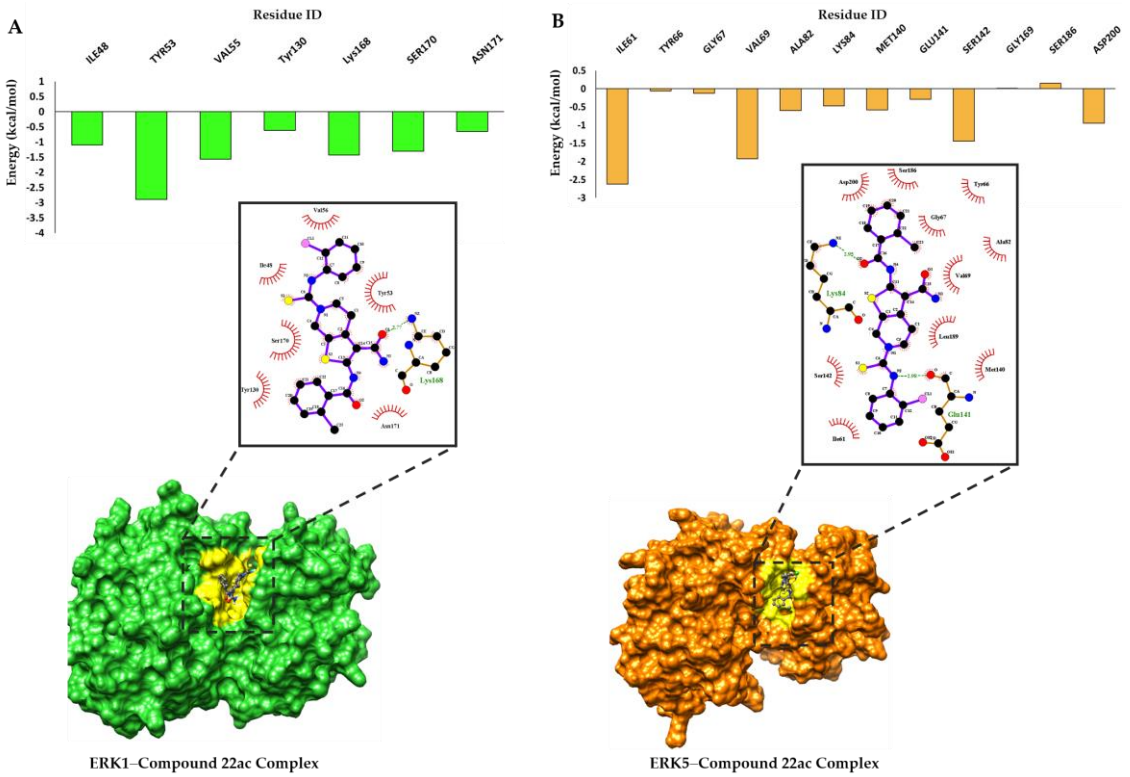

Figure 5. Per-residue energy contributions (PRED) of the interacting backbone residues at the ERK1 (**A**) and ERK5 (**B**) binding sites. Also shown are the significant protein–ligand interactions at the binding site of both proteins.

3.7. Residual Hydrogen Bond Contributions before and after MD Simulation

We evaluated the binding interactions of the complex structure of Compound 22ac against the two enzymes before and after MD simulation using snapshots. This analysis was conducted to emphasize the influence of H-bonds on the interactions established following the initial docking process, which only highlights the geometric fit of the ligand to the activity of the enzymes and molecular dynamics (MD) simulations. As shown in Figure 6, we discovered that the initial binding of Compound 22ac to ERK1 allows for at least two hydrogen bond interactions per snapshot taken, with major H-bond contributions from amino acid residues Glu50 and Asn171. These hydrogen bond interactions are mainly formed through interactions of the aforementioned amino acid residues with the -NH2 functional group attached to the 2-amino-3-carboxamide-thieno scaffold. However, other residues such as Ala69, Val56, Leu173, Asp128, and Lys131 also formed other interactions such as Pi-alkyl, Pi-sulfur, and alkyl interactions, as shown in Figure 5A. Comparatively, after simulation, only one H-bond was observed with Lys168 and an oxygen atom located at the 2-amino-3-carboxamide-thieno scaffold, although other interactions were observed with residues in the ATP hinge-binding domain.

Similarly, in the binding of Compound 22ac to ERK5, one (1) initial H-bond was observed with Asp200 at the ortho-chlorophenyl-thiourea moiety, as shown in Figure 5B, whereas after MD simulation, three H-bonds were formed with ASP138, Glu141, and Lys84 on the -NH2 functional group attached on the 2-amino-3-carboxamide-thieno scaffold and oxygen atom. Other interactions were also noted with key residues in the ATP hinge-binding domain. The different ligand orientations to achieve stability through dynamical simulation timeframes allowed for H-bond contributions from different residues on the ATP hinge region. In the process, initial interactions may be maintained or lost or new interactions may be formed during this conformational shift to attain stability. Hence, the additional H-bond interactions formed in the ERK5 complex and the loss of one H-bond interaction in the ERK1 complex. This possibly explains why the to-

tal energy contribution from ERK5 toward the binding affinity was higher than that of ERK1. This observation underscores the importance of H-bonding in the binding energy of protein–ligand complexes.

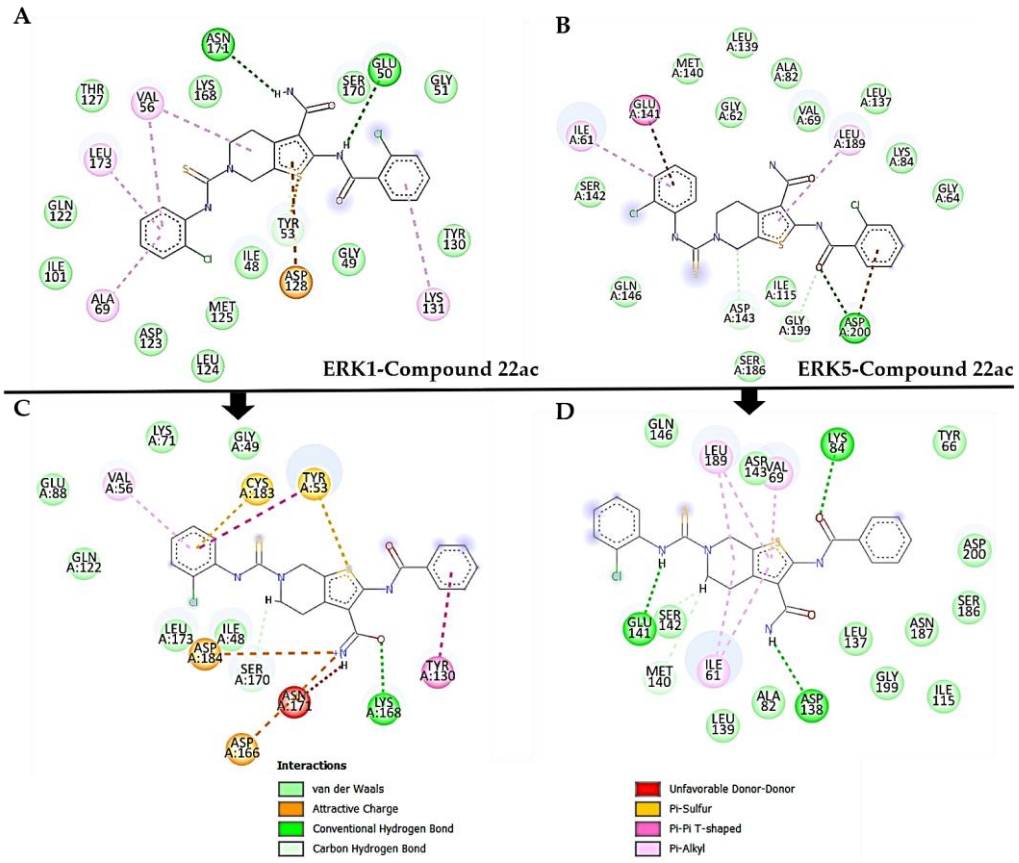

Figure 6. Snapshots showing H-bond interactions before and after MD simulation for the complex structure of Compound 22ac bound to ERK1 and ERK5. (**A**,**B**) depicting interactions before the simulation whiles (**C**,**D**) highlights interactions after simulation.

4. Discussion

In this current report, the structural and mechanistic activities that potentiate the dual inhibitory mechanism of Compound 22ac were highlighted using molecular dynamic simulations. Compound 22ac together with the selective ERK1 and ERK5 inhibitors SCH772984 and XMD8-92 were characterized using online predictive methods. The rule of five by Lipinski was considered in characterizing the inhibitors. The slightly higher molecular weight of Compound 22ac shows its violation of one descriptor of the rule of five, which is consequently reflected in its low GI absorption, as predicted; however, optimization can improve this parameter. All other parameters complied with the Lipinski standard, hence identifying them as bioavailable and potential to be used as oral drugs.

Furthermore, the reference drugs SCH-772984 and XMD8-92 were predicted to be substrates of the P-gp enzymes, implying they can be recognized and actively transported by P-gp out of cells. Compound 22ac, on the other hand, was identified as not being a substrate of the P-gp enzyme and hence, it may competitively or non-competitively bind to P-gp, thus preventing it from actively transporting its substrates. The primary function of CYP450 enzymes is to facilitate the biotransformation (metabolism) of drugs/compounds, making them more water-soluble and easier for the body to eliminate [68]. CYP3A4 is one of the most abundant and versatile CYP450 enzymes, which is responsible for metabolizing a significant proportion of drugs, including many commonly used medications. It is also prone to drug–drug interactions as it can be induced or inhibited by various

substances [69,70]. SCH-772984 and Compound 22ac were predicted to be inhibitors of CYP34A and may thus inhibit or slow the activity of the CYP3A4 enzyme. Whereas XMD8-92, which is not a CYP3A4 inhibitor, can easily be metabolized and eliminated from the body by the enzyme. Additionally, the synthetic accessibility score indicated that XMD8-92 can be easily synthesized, followed by Compound 22ac and then SCH-772984. This parameter is determined by a scale ranging from 1 (very easy to synthesize) to 10 (very difficult to synthesize) [64]. The toxicity assessment, as predicted using the Pro-Tox II server, classified all the inhibitors in a toxicity class IV, indicative of being less harmful [71]. Furthermore, Compound 22ac demonstrated an outstanding toxicity effect on the endpoints assessed by showing inactivity when administered at a lethal dosage. The reference SCH-772984 and XMD8-92 appear to be immunotoxic, cytotoxic, and carcinogenic at their lethal dosages. This variation in the predicted results for the inhibitors can be attributed to distinct structural features, where Compound 22ac comprises an ortho-chlorobenzamide (containing amide group) and 2-amin-3-carboxamide-thieno (containing H-N group) as prominent scaffolds/core structures, whereas SCH772984 and XMD8-92 have no distinct scaffolds but have functional groups such as amide, carbonyl, chlorine, and alkyl groups [72–74].

Subsequently, the structural and molecular mechanism of the dual inhibitory activity of Compound 22ac was analyzed using molecular dynamics simulations. The interactions between the residues in the protein and its xenobiotic were shown to be highly important in the role they play in biological functions. MD simulations help to determine motions that occur in a protein–ligand complex over a period of time. All simulated inhibitors stabilized the ERK enzymes, although the Compound 22ac-bound systems were the most stable. As reported in many studies, a unique characteristic of ERK inhibitors is their ability to stabilize the inactive state of a target, thus making it less likely to transition to an active state [72,75,76]. Also, Compound 22ac was able to enact significant residual flexibility on both enzymes, thereby inducing a conformational change. Some ERK inhibitors work by inducing conformational changes in the kinase, which is a mechanism that results in the kinase adopting an inactive conformation that is unable to phosphorylate substrates. Overall, the analysis of the structural dynamics of the binding of Compound 22ac unveils significant conformational changes that can hinder the kinase's activity and prevent it from phosphorylating its substrates, thereby disrupting the cellular signaling pathways in which ERK1 and ERK5 are involved. This disruption may have therapeutic applications, particularly in the context of cancer or other diseases where aberrant ERK1/5 activity plays a role.

We delved deeper into the thermodynamic binding mechanism of Compound 22ac with a specific focus on understanding the residence times and the specific interactions occurring between this compound and the ERK1 and ERK5 enzymes. Our investigation revealed significant insights into the binding dynamics and the thermodynamic favorability of these interactions, aligning with recent experimental findings.

Our computational analysis unveiled that the total free energy and interaction of Compound 22ac in complex with ERK5 was highly favorable. In comparison, when bound to the ERK1 complex, the total free energy was marginally lower, although it still suggested a favorable binding affinity. This divergence in binding energies closely mimics the experimental data reported by Guan et al., who conducted kinase inhibitory assays. In their work, they determined the IC_{50} values for Compound 22ac against ERK1 and ERK5 to be 40.43 nM and 64.50 nM, respectively [26].

The observed discrepancy between the IC_{50} values of Compound 22ac for ERK1 and ERK5 and the corresponding free energy values may be attributed to the multifaceted nature of binding interactions. While IC_{50} values summarize the effective concentration of Compound 22ac required to inhibit the enzymatic activity by 50% [77], our free energy calculations consider the thermodynamic factors governing binding, such as van der Waals interactions, electrostatic forces, hydrogen bonding, and solvation contributions [78,79]. Hence, they provide a more detailed view of the energetic landscape of these interactions elicited by Compound 22ac toward the two targets. Also, the minimal energy differences

and the consistency in energy profiles across both ERK1 and ERK5 complexes hint at the likelihood of Compound 22ac binding to conserved motifs of the two enzymes. This hypothesis aligns with the principle of dual inhibition, where a single compound can effectively modulate the activity of multiple enzymes or targets by leveraging shared structural features [80].

Furthermore, when the free energy of Compound 22ac was compared to that of SCH-772984 and XMD8-92, which are established as specific inhibitors for their respective targets, the calculated free energy values were notably similar. This finding draws significant attention regarding the compound's selectivity and its potential role as a versatile modulator in the MAPK signaling pathway. Compound 22ac has been shown to reduce ERK1 and ERK5 activity by 93.5% and 89.4%, based on *in vitro* assays, respectively; inhibit proliferation of HL-60 and MKN74 cancers; and reduce tumor growth and intratumor phosphorylation of ERK1/2 and ERK5 in an MKN74 mouse xenograft model [26]. Therefore, the findings from this study complement experimental assays by providing novel insights into the molecular mechanism of its dual inhibition via *in silico* means.

5. Conclusions

This report provides a comprehensive exploration of the structural and mechanistic insights into the dual inhibition activity of Compound 22ac toward two pivotal enzymes, ERK1 and ERK5, within the intricate MAPK signaling pathway. The discovery of this dual inhibition mechanism offers valuable contributions to our understanding of molecular interactions and drug design strategies. Understanding how Compound 22ac can effectively modulate both ERK1 and ERK5 simultaneously not only sheds light on the fundamental biological processes underlying MAPK signaling but also holds promise for various therapeutic applications. This dual-inhibitor approach presents numerous advantages, ranging from enhanced treatment efficacy to the potential mitigation of drug resistance, making it a compelling avenue for drug development and precision medicine. As we delve deeper into the intricacies of molecular mechanisms, the knowledge derived from this research can pave the way for the design of more potent and selective therapeutic agents, offering patients more efficient and tailored treatment options. This report exemplifies the ongoing pursuit of innovative strategies in the field of pharmacology and molecular biology, emphasizing the importance of dual inhibition as a versatile and promising approach to addressing complex diseases and advancing the frontiers of medical science.

Supplementary Materials: The following supporting information can be downloaded at: https://www.mdpi.com/article/10.3390/computation12030045/s1, Figure S1: Per-residue energy contributions (PRED) of the interacting backbone residues at ERK1 [A] and ERK5 [B] binding sites against SCH-772984 and XMD8-92. Also shown is the significant protein-ligand interactions at the binding site of both proteins.

Author Contributions: Conceptualization, E.Y.S.; methodology, E.Y.S.; formal analysis, E.Y.S.; writing—original draft, E.Y.S., P.R. and M.A.F.; writing—review and editing, P.R., E.Y.S., M.A.F. and J.A. All authors have read and agreed to the published version of the manuscript.

Funding: This research was funded by a National Research Foundation Postdoctoral Fellowship Grant (grant number: 50632), the National Research Foundation Thuthuka grant (grant number: 138392) and the South African Medical Research Council (SAMRC) Biomedical and Research Innovation Platform (BRIP).

Data Availability Statement: The data are contained within this article and the Supplementary Materials.

Acknowledgments: The authors would like to acknowledge the National Integrated Cyberinfrastructure System's Centre for High-Performance Computing (NICIS-CHPC) for the computing resources required for this study.

Conflicts of Interest: The authors declare no conflicts of interest.

References

1. Guo, Y.; Pan, W.; Liu, S.; Shen, Z.; Xu, Y.; Hu, L. ERK/MAPK signalling pathway and tumorigenesis (Review). *Exp. Ther. Med.* **2020**, *19*, 1997–2007. [CrossRef]
2. Schaeffer, H.J.; Weber, M.J. Mitogen-Activated Protein Kinases: Specific Messages from Ubiquitous Messengers. *Mol. Cell. Biol.* **1999**, *19*, 2435–2444. [CrossRef] [PubMed]
3. Kumar, S.; Principe, D.R.; Singh, S.K.; Viswakarma, N.; Sondarva, G.; Rana, B.; Rana, A. Mitogen-activated protein kinase inhibitors and T-cell-dependent immunotherapy in cancer. *Pharmaceuticals* **2020**, *13*, 9. [CrossRef]
4. Gaestel, M. MAPK-activated protein kinases (MKs): Novel insights and challenges. *Front. Cell Dev. Biol.* **2016**, *3*, 88. [CrossRef] [PubMed]
5. Huang, C.; Jacobson, K.; Schaller, M.D. MAP kinases and cell migration. *J. Cell Sci.* **2004**, *117*, 4619–4628. [CrossRef] [PubMed]
6. Keshet, Y.; Seger, R. The MAP Kinase Signaling Cascades: A System of Hundreds of Components Regulates a Diverse Array of Physiological Functions. *Methods Mol. Biol.* **2010**, *661*, 3–38. [CrossRef] [PubMed]
7. Sabio, G.; Davis, R.J. TNF and MAP kinase signalling pathways. *Semin. Immunol.* **2014**, *26*, 237–245. [CrossRef] [PubMed]
8. Plotnikov, A.; Zehorai, E.; Procaccia, S.; Seger, R. The MAPK cascades: Signaling components, nuclear roles and mechanisms of nuclear translocation. *Biochim. Biophys. Acta Mol. Cell Res.* **2011**, *1813*, 1619–1633. [CrossRef] [PubMed]
9. Eblen, S.T. *Extracellular-Regulated Kinases: Signaling from Ras to ERK Substrates to Control Biological Outcomes*, 1st ed.; Elsevier: Amsterdam, The Netherlands, 2018; Volume 138.
10. Seternes, O.M.; Kidger, A.M.; Keyse, S.M. Dual-specificity MAP kinase phosphatases in health and disease. *Biochim. Biophys. Acta Mol. Cell Res.* **2019**, *1866*, 124–143. [CrossRef]
11. Sun, Y.; Liu, W.Z.; Liu, T.; Feng, X.; Yang, N.; Zhou, H.F. Signaling pathway of MAPK/ERK in cell proliferation, differentiation, migration, senescence and apoptosis. *J. Recept. Signal Transduct.* **2015**, *35*, 600–604. [CrossRef]
12. Kyosseva, S.V. Mitogen-activated protein kinase signaling. *Int. Rev. Neurobiol.* **2004**, *59*, 201–220. [CrossRef] [PubMed]
13. Soares-Silva, M.; Diniz, F.F.; Gomes, G.N.; Bahia, D. The mitogen-activated protein kinase (MAPK) pathway: Role in immune evasion by trypanosomatids. *Front. Microbiol.* **2016**, *7*, 183. [CrossRef] [PubMed]
14. Trott, O.; Olson, A.J. Autodock vina: Improving the speed and accuracy of docking. *J. Comput. Chem.* **2010**, *31*, 455–461. [CrossRef] [PubMed]
15. Kidger, A.M.; Munck, J.M.; Saini, H.K.; Balmanno, K.; Minihane, E.; Courtin, A.; Graham, B.; O'Reilly, M.; Odle, R.; Cook, S.J. Dual-mechanism ERK1/2 inhibitors exploit a distinct binding mode to block phosphorylation and nuclear accumulation of ERK1/2. *Mol. Cancer Ther.* **2020**, *19*, 525–539. [CrossRef] [PubMed]
16. Sohn, S.J.; Sarvis, B.K.; Cado, D.; Winoto, A. ERK5 MAPK regulates embryonic angiogenesis and acts as a hypoxia-sensitive repressor of vascular endothelial growth factor expression. *J. Biol. Chem.* **2002**, *277*, 43344–43351. [CrossRef] [PubMed]
17. Krueger, J.S.; Keshamouni, V.G.; Atanaskova, N.; Reddy, K.B. Temporal and quantitative regulation of mitogen-activated protein kinase (MAPK) modulates cell motility and invasion. *Oncogene* **2001**, *20*, 4209–4218. [CrossRef]
18. Hickson, J.A.; Huo, D.; Vander Griend, D.J.; Lin, A.; Rinker-Schaeffer, C.W.; Yamada, S.D. The p38 kinases MKK4 and MKK6 suppress metastatic colonization in human ovarian carcinoma. *Cancer Res.* **2006**, *66*, 2264–2270. [CrossRef]
19. Wada, T.; Penninger, J.M. Mitogen-activated protein kinases in apoptosis regulation. *Oncogene* **2004**, *23*, 2838–2849. [CrossRef]
20. Tibbles, L.A.; Woodgett, J.R. The stress-activated protein kinase pathways. *Cell. Mol. Life Sci.* **1999**, *55*, 1230–1254. [CrossRef]
21. Johnson, G.L.; Lapadat, R. Mitogen-activated protein kinase pathways mediated by ERK, JNK, and p38 protein kinases. *Science* **2002**, *298*, 1911–1912. [CrossRef]
22. Chang, L.; Karin, M. Mammalian MAP kinase signalling cascades. *Nature* **2001**, *410*, 37–40. [CrossRef] [PubMed]
23. Seger, R.; Krebs, E.G. The MAPK signaling Cascade. *FASEB J.* **1995**, *9*, 726–735. [CrossRef] [PubMed]
24. Lochhead, P.A.; Tucker, J.A.; Tatum, N.J.; Wang, J.; Oxley, D.; Kidger, A.M.; Johnson, V.P.; Cassidy, M.A.; Gray, N.S.; Cook, S.J.; et al. Paradoxical activation of the protein kinase-transcription factor ERK5 by ERK5 kinase inhibitors. *Nat. Commun.* **2020**, *11*, 1383. [CrossRef] [PubMed]
25. De Jong, P.R.; Taniguchi, K.; Harris, A.R.; Bertin, S.; Takahashi, N.; Duong, J.; Campos, A.D.; Powis, G.; Corr, M.; Raz, E.; et al. ERK5 signalling rescues intestinal epithelial turnover and tumour cell proliferation upon ERK1/2 abrogation. *Nat. Commun.* **2016**, *7*, 11551. [CrossRef] [PubMed]
26. Zhang, W.; Liu, H.T. MAPK signal pathways in the regulation of cell proliferation in mammalian cells. *Cell Res.* **2002**, *12*, 9–18. [CrossRef]
27. Samadani, R.; Zhang, J.; Brophy, A.; Oashi, T.; Priyakumar, U.D.; Raman, E.P.; John, F.J.S.; Jung, K.Y.; Fletcher, S.; Pozharski, E.; et al. Small-molecule inhibitors of ERK-mediated immediate early gene expression and proliferation of melanoma cells expressing mutated BRaf. *Biochem. J.* **2015**, *467*, 425–438. [CrossRef] [PubMed]
28. Lu, N.; Malemud, C.J. Extracellular signal-regulated kinase: A regulator of cell growth, inflammation, chondrocyte and bone cell receptor-mediated gene expression. *Int. J. Mol. Sci.* **2019**, *20*, 3792. [CrossRef] [PubMed]
29. Drew, B.A.; Burow, M.E.; Beckman, B.S. MEK5/ERK5 pathway: The first fifteen years. *Biochim. Biophys. Acta Rev. Cancer* **2012**, *1825*, 37–48. [CrossRef]
30. Wang, G.; Zhao, Y.; Liu, Y.; Sun, D.; Zhen, Y.; Liu, J.; Fu, L.; Zhang, L.; Ouyang, L. Discovery of a Novel Dual-Target Inhibitor of ERK1 and ERK5 That Induces Regulated Cell Death to Overcome Compensatory Mechanism in Specific Tumor Types. *J. Med. Chem.* **2020**, *63*, 3976–3995. [CrossRef]

31. Kato, Y.; Tapping, R.I.; Huang, S.; Watson, M.H.; Ulevitch, R.J.; Lee, J.-D. Bmk1/Erk5 is required for cell proliferation induced byepidermalgrowth factor. *Nature* **1998**, *395*, 713–716. [CrossRef]
32. Pearson, G.; English, J.M.; White, M.A.; Cobb, M.H. ERK5 and ERK2 Cooperate to Regulate NF-κB and Cell Transformation. *J. Biol. Chem.* **2001**, *276*, 7927–7931. [CrossRef] [PubMed]
33. Nishimoto, S.; Nishida, E. MAPK signalling: ERK5 versus ERK1/2. *EMBO Rep.* **2006**, *7*, 782–786. [CrossRef] [PubMed]
34. Zdanov, S.; Mandapathil, M.; Eid, R.A.; Adamson-Fadeyi, S.; Wilson, W.; Qian, J.; Carnie, A.; Tarasova, N.; Mkrtichyan, M.; Berzofsky, J.A.; et al. Mutant KRAS conversion of conventional T cells into regulatory T cells. *Cancer Immunol. Res.* **2016**, *4*, 354–365. [CrossRef]
35. Hoang, V.T.; Yan, T.J.; Cavanaugh, J.E.; Flaherty, P.T.; Beckman, B.S.; Burow, M.E. Oncogenic signaling of MEK5-ERK5. *Cancer Lett.* **2017**, *392*, 51–59. [CrossRef]
36. Kopecka, J.; Porto, S.; Lusa, S.; Gazzano, E.; Salzano, G.; Pinzòn-Daza, M.L.; Giordano, A.; Desiderio, V.; Ghigo, D.; De Rosa, G.; et al. Zoledronic acid-encapsulating self-assembling nanoparticles and doxorubicin: A combinatorial approach to overcome simultaneously chemoresistance and immunoresistance in breast tumors. *Oncotarget* **2016**, *7*, 20753–20772. [CrossRef]
37. Liu, Z.; Zhao, Y.; Fang, J.; Cui, R.; Xiao, Y.; Xu, Q. SHP2 negatively regulates HLA-ABC and PD-L1 expression via STAT1 phosphorylation in prostate cancer cells. *Oncotarget* **2017**, *8*, 53518–53530. [CrossRef]
38. Salaroglio, I.C.; Campia, I.; Kopecka, J.; Gazzano, E.; Sara, O.; Ghigo, D.; Riganti, C. Zoledronic acid overcomes chemoresistance and immunosuppression of malignant mesothelioma. *Oncotarget* **2015**, *6*, 1128–1142. [CrossRef]
39. Chen, N.; Fang, W.; Lin, Z.; Peng, P.; Wang, J.; Zhan, J.; Hong, S.; Huang, J.; Liu, L.; Sheng, J.; et al. KRAS mutation-induced upregulation of PD-L1 mediates immune escape in human lung adenocarcinoma. *Cancer Immunol. Immunother.* **2017**, *66*, 1175–1187. [CrossRef]
40. Tan, B.; Shi, X.; Zhang, J.; Qin, J.; Zhang, N.; Ren, H.; Qian, M.; Siwko, S.; Carmon, K.; Liu, Q.; et al. Inhibition of RSPO-LGR4 facilitates checkpoint blockade therapy by switching macrophage polarization. *Cancer Res.* **2018**, *78*, 4929–4942. [CrossRef]
41. Xing, Y.N.; Zhang, J.Y.; Xu, H.M. The roles of serum CXCL16 in circulating Tregs and gastrointestinal stromal tumor cells. *Onco. Targets. Ther.* **2016**, *9*, 3939–3949. [CrossRef] [PubMed]
42. Qiu, X.Y.; Hu, D.X.; Chen, W.Q.; Chen, R.Q.; Qian, S.R.; Li, C.Y.; Li, Y.J.; Xiong, X.X.; Liu, D.; Pan, F.; et al. PD-L1 confers glioblastoma multiforme malignancy via Ras binding and Ras/Erk/EMT activation. *Biochim. Biophys. Acta Mol. Basis Dis.* **2018**, *1864*, 1754–1769. [CrossRef]
43. Ho, V.; Lim, T.S.; Lee, J.; Steinberg, J.; Szmyd, R.; Tham, M.; Yaligar, J.; Kaldis, P.; Abastado, J.P.; Chew, V. TLR3 agonist and Sorafenib combinatorial therapy promotes immune activation and controls hepatocellular carcinoma progression. *Oncotarget* **2015**, *6*, 27252–27266. [CrossRef]
44. Li, Y.; Yang, Q. Effect of PD98059 on chemotherapy in patients with colorectal cancer through ERK1/2 pathway. *J. BUON* **2019**, *24*, 1837–1844.
45. Tian, P.; Zhu, Y.; Zhang, C.; Guo, X.; Zhang, P.; Xue, H. Ras-ERK1/2 signaling contributes to the development of colorectal cancer via regulating H3K9ac. *BMC Cancer* **2018**, *18*, 1286. [CrossRef] [PubMed]
46. Yan, Z.; Ohuchida, K.; Fei, S.; Zheng, B.; Guan, W.; Feng, H.; Kibe, S.; Ando, Y.; Koikawa, K.; Abe, T.; et al. Inhibition of ERK1/2 in cancer-associated pancreatic stellate cells suppresses cancer-stromal interaction and metastasis. *J. Exp. Clin. Cancer Res.* **2019**, *38*, 221. [CrossRef] [PubMed]
47. Simões, A.E.S.; Rodrigues, C.M.P.; Borralho, P.M. The MEK5/ERK5 signalling pathway in cancer: A promising novel therapeutic target. *Drug Discov. Today* **2016**, *21*, 1654–1663. [CrossRef]
48. Stecca, B.; Rovida, E. Impact of ERK5 on the hallmarks of cancer. *Int. J. Mol. Sci.* **2019**, *20*, 1426. [CrossRef]
49. Pettersen, E.F.; Goddard, T.D.; Huang, C.C.; Couch, G.S.; Greenblatt, D.M.; Meng, E.C.; Ferrin, T.E. UCSF Chimera—A visualization system for exploratory research and analysis. *J. Comput. Chem.* **2004**, *25*, 1605–1612. [CrossRef]
50. Yang, Z.; Lasker, K.; Schneidman-Duhovny, D.; Webb, B.; Huang, C.C.; Pettersen, E.F.; Goddard, T.D.; Meng, E.C.; Sali, A.; Ferrin, T.E. UCSF Chimera, MODELLER, and IMP: An integrated modeling system. *J. Struct. Biol.* **2012**, *179*, 269–278. [CrossRef] [PubMed]
51. Webb, B.; Sali, A. Comparative protein structure modeling using MODELLER. *Curr. Protoc. Bioinforma.* **2016**, *2016*, 5.6.1–5.6.37. [CrossRef]
52. Cherinka, B.; Andrews, B.H.; Sánchez-Gallego, J.; Brownstein, J.; Argudo-Fernández, M.; Blanton, M.; Bundy, K.; Jones, A.; Masters, K.; Law, D.R.; et al. Marvin: A Tool Kit for Streamlined Access and Visualization of the SDSS-IV MaNGA Data Set. *Astron. J.* **2019**, *158*, 74. [CrossRef]
53. Hanwell, M.D.; Curtis, D.E.; Lonie, D.C.; Vandermeersch, T.; Zurek, E.; Hutchison, G.R. Avogadro: An advanced semantic chemical editor, visualization, and analysis platform. *J. Cheminform.* **2012**, *4*, 17. [CrossRef]
54. Allouche, A. Software News and Updates Gabedit—A Graphical User Interface for Computational Chemistry Softwares. *J. Comput. Chem.* **2012**, *32*, 174–182. [CrossRef]
55. Case, D.A.; Walker, R.C.; Cheatham, T.E.; Simmerling, C.; Roitberg, A.; Merz, K.M.; Luo, R.; Darden, T. *Amber 18*; University of California: San Francisco, CA, USA, 2018.
56. Maier, J.A.; Martinez, C.; Kasavajhala, K.; Wickstrom, L.; Hauser, K.E.; Simmerling, C. ff14SB: Improving the Accuracy of Protein Side Chain and Backbone Parameters from ff99SB. *J. Chem. Theory Comput.* **2015**, *11*, 3696–3713. [CrossRef] [PubMed]

57. Case, D.A.; Cheatham, T.E.; Darden, T.; Gohlke, H.; Luo, R.; Merz, K.M.; Onufriev, A.; Simmerling, C.; Wang, B.; Woods, R.J. The Amber biomolecular simulation programs. *J. Comput. Chem.* **2005**, *26*, 1668–1688. [CrossRef]
58. Jorgensen, W.L.; Chandrasekhar, J.; Madura, J.D.; Impey, R.W.; Klein, M.L. Comparison of simple potential functions for simulating liquid water. *J. Chem. Phys.* **1983**, *79*, 926–935. [CrossRef]
59. Berendsen, H.J.C.; Postma, J.P.M.; van Gunsteren, W.F.; DiNola, A.; Haak, J.R. Molecular dynamics with coupling to an external bath. *J. Chem. Phys.* **1984**, *81*, 3684–3690. [CrossRef]
60. Roe, D.R.; Cheatham, T.E. PTRAJ and CPPTRAJ: Software for Processing and Analysis of Molecular Dynamics Trajectory Data. *J. Chem. Theory Comput.* **2013**, *9*, 3084–3095. [CrossRef] [PubMed]
61. Seifert, E. OriginPro 9.1: Scientific data analysis and graphing software—Software review. *J. Chem. Inf. Model.* **2014**, *54*, 1552. [CrossRef] [PubMed]
62. Kollman, P.A.; Massova, I.; Reyes, C.; Kuhn, B.; Huo, S.; Chong, L.; Lee, M.; Lee, T.; Duan, Y.; Wang, W.; et al. Calculating structures and free energies of complex molecules: Combining molecular mechanics and continuum models. *Acc. Chem. Res.* **2000**, *33*, 889–897. [CrossRef]
63. Daina, A.; Michielin, O.; Zoete, V. SwissADME: A free web tool to evaluate pharmacokinetics, drug-likeness and medicinal chemistry friendliness of small molecules. *Sci. Rep.* **2017**, *7*, 42717. [CrossRef]
64. Schweppe, R.E.; Tom, H.C.; Ahn, N.G. Global gene expression analysis of ERK5 and ERK1/2 signaling reveals a role for HIF-1 in ERK5-mediated responses. *J. Biol. Chem.* **2006**, *281*, 20993–21003. [CrossRef]
65. Bös, F.; Pleiss, J. Multiple molecular dynamics simulations of TEM β-lactamase: Dynamics and water binding of the Ω-loop. *Biophys. J.* **2009**, *97*, 2550–2558. [CrossRef]
66. Sousa Da Silva, A.W.; Vranken, W.F. ACPYPE—AnteChamber PYthon Parser interface. *BMC Res. Notes* **2012**, *5*, 367. [CrossRef]
67. Fatunde, O.A.; Brown, S.A. The role of CYP450 drug metabolism in precision Cardio-Oncology. *Int. J. Mol. Sci.* **2020**, *21*, 604. [CrossRef]
68. Kiani, Y.S.; Ranaghan, K.E.; Jabeen, I.; Mulholland, A.J. Molecular dynamics simulation framework to probe the binding hypothesis of CYP3A4 inhibitors. *Int. J. Mol. Sci.* **2019**, *20*, 4468. [CrossRef] [PubMed]
69. Kondža, M.; Bojić, M.; Tomić, I.; Maleš, Ž.; Rezić, V.; Ćavar, I. Characterization of the cyp3a4 enzyme inhibition potential of selected flavonoids. *Molecules* **2021**, *26*, 3018. [CrossRef] [PubMed]
70. Banerjee, P.; Eckert, A.O.; Schrey, A.K.; Preissner, R. ProTox-II: A webserver for the prediction of toxicity of chemicals. *Nucleic Acids Res.* **2018**, *46*, W257–W263. [CrossRef]
71. Chaikuad, A.; Tacconi, E.M.C.; Zimmer, J.; Liang, Y.; Gray, N.S.; Tarsounas, M.; Knapp, S. A unique inhibitor binding site in ERK1/2 is associated with slow binding kinetics. *Nat. Chem. Biol.* **2014**, *10*, 853–860. [CrossRef] [PubMed]
72. Kopczynski, M.; Rumienczyk, I.; Kulecka, M.; Statkiewicz, M.; Pysniak, K.; Sandowska-Markiewicz, Z.; Wojcik-Trechcinska, U.; Goryca, K.; Pyziak, K.; Majewska, E.; et al. Selective extracellular signal-regulated kinase 1/2 (ERK1/2) inhibition by the SCH772984 compound attenuates in vitro and in vivo inflammatory responses and prolongs survival in murine sepsis models. *Int. J. Mol. Sci.* **2021**, *22*, 204. [CrossRef]
73. Kang, C.; Kim, J.S.; Kim, C.Y.; Kim, E.Y.; Chung, H.M. The pharmacological inhibition of ERK5 enhances apoptosis in acute myeloid leukemia cells. *Int. J. Stem Cells* **2018**, *11*, 227–234. [CrossRef] [PubMed]
74. Sammons, R.M.; Ghose, R.; Tsai, K.Y.; Dalby, K.N. Targeting ERK beyond the boundaries of the kinase active site in melanoma. *Mol. Carcinog.* **2019**, *58*, 1551–1570. [CrossRef] [PubMed]
75. Rudolph, J.; Xiao, Y.; Pardi, A.; Ahn, N.G. Slow inhibition and conformation selective properties of extracellular signal-regulated kinase 1 and 2 inhibitors. *Biochemistry* **2015**, *54*, 22–31. [CrossRef] [PubMed]
76. Sebaugh, J.L. Guidelines for accurate EC50/IC50 estimation. *Pharm. Stat.* **2011**, *10*, 128–134. [CrossRef] [PubMed]
77. Blumberger, J. Free energies for biological electron transfer from QM/MM calculation: Method, application and critical assessment. *Phys. Chem. Chem. Phys.* **2008**, *10*, 5651–5667. [CrossRef] [PubMed]
78. Gilson, M.K.; Zhou, H.X. Calculation of protein-ligand binding affinities. *Annu. Rev. Biophys. Biomol. Struct.* **2007**, *36*, 21–42. [CrossRef]
79. Babu, P.A.; Chitti, S.; Rajesh, B.; Prasanth, V.V.; Kishen JV, R.; Vali, R.K. In silico based ligand design and docking studies of GSK-3β inhibitors. *Chem-Bio Inform. J.* **2010**, *10*, 1–12. [CrossRef]
80. Patyar, S.; Prakash, A.; Medhi, B. Dual inhibition: A novel promising pharmacological approach for different disease conditions. *J. Pharm. Pharmacol.* **2011**, *63*, 459–471. [CrossRef]